

Journal of Biomedical Optics

SPIEDigitalLibrary.org/jbo

Possibilities of optical imaging of the ^{99m}Tc -based radiopharmaceuticals

Anton K. Kondakov
Ilya L. Gubskiy
Igor A. Znamenskiy
Vladimir P. Chekhonin



SPIE

Possibilities of optical imaging of the ^{99m}Tc -based radiopharmaceuticals

Anton K. Kondakov,^{a,*} Ilya L. Gubskiy,^b Igor A. Znamenskiy,^{a,c} and Vladimir P. Chekhonin^{b,d}

^aPirogov Russian National Research Medical University, Department of Radiology and Radiotherapy, 1 Ostrovityanova Street, Moscow 117997, Russian Federation

^bPirogov Russian National Research Medical University, Department of Medical Nanobiotechnology, 1 Ostrovityanova Street, Moscow 117997, Russian Federation

^cCentral Clinical Hospital of the Russian Academy of Sciences, 12 b.3 Fotievoy Street, Moscow 119333, Russian Federation

^dSerbsky State Research Center of Social and Forensic Psychiatry, Division of Fundamental and Applied Neurobiology, 23 b.2 Kropotkinskiy per., Moscow 119034, Russian Federation

Abstract. *In vivo* optical imaging is widely used in preclinical studies. Recently, the application of optical imaging systems for preclinical visualization of gamma-emitting isotopes has become of interest since the evaluation of various organs relies on ^{99m}Tc -based radiopharmaceuticals (RPs). *In vitro* radioluminescence of ^{99m}Tc -based RPs, including pertechnetate, albumin macroaggregates, dimercaptosuccinic acid, phytate colloid, and ethylenediamine tetramethylene phosphonic acid, was studied with IVIS Spectrum CT™ optical imaging system. The distribution of phytate colloid was also studied *in vivo* with and without scintillating materials and the results were compared with those obtained with a conventional scintigraphy. The visible light emission appeared to be due to the radioluminescence of water and luminophores contained in RPs rather than from Cherenkov radiation. Weak air luminescence affected the background. The radioluminescence of fluids induced by ^{99m}Tc -based tracers could be detected using charge-coupled device optical imaging systems. The radioluminescence intensity and its spectral distribution depend on the surrounding fluid and known luminophores present. Thus, in some cases the *in vivo* optical imaging is possible but the use of scintillator, e.g., borosilicate glass or bismuth germanate, is preferred. © 2014 Society of Photo-Optical Instrumentation Engineers (SPIE) [DOI: 10.1117/1.JBO.19.4.046014]

Keywords: optical imaging; radiopharmaceuticals; radioluminescence; technetium-99m; small animal; Cherenkov radiation.

Paper 140066R received Feb. 3, 2014; revised manuscript received Mar. 22, 2014; accepted for publication Mar. 25, 2014; published online Apr. 21, 2014.

1 Background

Radioisotope imaging is a sensitive and noninvasive method for the evaluation of functional changes in organs by means of the administration of small amounts of radioactive compounds. The emergence of new types of radiopharmaceuticals (RPs) drives further developments in this field of nuclear medicine. Gamma-cameras and positron-emitting tomography scanners for the small animals are currently used for the evaluation of RP distribution.¹

The use of optical imaging in the preclinical studies of RP distribution, including those used for ^{99m}Tc -based RPs, has been suggested by several investigators.

The isotope optical imaging has been first introduced by Robertson et al.,² who used positron-emitting isotopes with the *in vivo* optical imaging systems IVIS 100™ and IVIS 200™ (Caliper Life Sciences, Texas) and determined characteristics of resulting electromagnetic radiation in the visible range. The measured intensity of the visible light emission from isotopes of ^{18}F and ^{13}N has been established to be proportional to the reciprocal of its wavelength squared ($1/\lambda^2$), and also proportional to the refractive index. These findings led the authors to conclude that the visible light observed is a Cherenkov radiation (CR), which is induced by positrons traveling through media with a velocity greater than the speed of light. This

type of radiation was discovered by Russian scientists P. A. Cherenkov and S. I Vavilov in the 1930s.^{3,4}

Spinelli et al.⁵ came to the same conclusions, investigating the depth of the radioactive source in the soft tissues and pharmacokinetics of the RP. The physical model of CR, proposed by Spinelli et al., is discussed in paper by Mitchell et al.⁶ The CR from positron-emitting RP has been addressed in following publications by Thorek et al.,⁷ Xu et al.,^{8–10} Lucignani,¹¹ Spinelli et al.,^{12,13} and Dothager et al.¹⁴

^{99m}Tc is a widely used medical isotope for scintigraphy and single-photon emission tomography (SPECT) due to its excellent physical properties and complex-forming abilities. Recently, new ^{99m}Tc -based RPs have become available, including monoclonal antibodies¹⁵ and tilmanocept.¹⁶

^{99m}Tc is virtually a pure gamma-emitting isotope with a half-life of 6 h and photon energy of 140 keV (99%) and 142 keV (1%). It decays by isomeric transition to ^{99}Tc or with the extremely low probability (0.000026%) through beta-decay to stable ^{99}Ru .¹⁷

Both in preclinical and clinical investigations, ^{99m}Tc -based RP has been visualized with an Anger camera or SPECT. However, the recent research has shown feasibility of the optical imaging for ^{99m}Tc -based RP visualizations. In particular, Spinelli et al.¹⁸ suggest the optical imaging as a cheaper alternative for small animals' Anger cameras.

*Address all correspondence to: Anton K. Kondakov, E-mail: kondakov.a.k@gmail.com

On the other hand, there are a number of papers including Xu et al.,¹⁰ Robertson et al.,² and Liu et al.,¹⁹ report no optical emission due to ^{99m}Tc .

The first study investigating optical imaging of the technetium-based tracer distribution in small animals was performed by Boschi et al.²⁰ The authors have used the known scintillator, bismuth germanate crystals, for optical visualization of gamma-photons emission.

Spinelli et al.¹⁸ also showed that optical imaging of the ^{99m}Tc -RP is possible even without any scintillating material. Moreover, the intensity of this light emission is decreasing with a half-life about 6 h, coincident with the decay of ^{99m}Tc . The paper discusses the soft tissue visualization along with pharmacokinetics of a ^{99m}Tc -based radiotracer for bone tissue, methylene diphosphonate (MDP). It was shown that accumulation of ^{99m}Tc -MDP in bladder can be clearly visualized after its intravenous injection in the tail vein of animal. The authors suggest two possible explanations for the light emission mechanisms: (1) Cherenkov light emission due to extremely weak ^{99m}Tc beta-decay or (2) non-Cherenkov light emission named as “radioluminescence” (RL).

Further studies of the ^{99m}Tc RL were conducted by Boschi et al.²¹ The authors studied the ^{99m}Tc -pertechnetate uptake in thyroid, salivary glands, and stomach of the nude mice. Obvious differences of the uptake patterns between ^{99m}Tc -pertechnetate and ^{99m}Tc -MDP demonstrated that optical imaging could be used in the evaluation of the thyroid function of small animals with ^{99m}Tc -pertechnetate.

Our work is to assess feasibility of RL imaging both *in vivo* and *in vitro* for the different RP and spectral characteristic of such luminescence.

2 Materials and Methods

The *In vivo* imaging system IVIS Spectrum CTTM (Caliper Life Sciences, Hopkinton, Massachusetts) was used for both *in vivo* and *in vitro* imaging of RL. The bioluminescent option was used in all experiments. The image acquisition parameters, such as, binning (B), focal ratio (f -number), field-of-view (FOV), exposition and emission filter used, are specified in the descriptions of experiments below. The image analysis was performed with Living Image 4.4TM (Caliper Life Sciences).

Conventional scintigraphy and SPECT studies were performed using Infinia Hawkeye 4TM (General Electric, Milwaukee, Wisconsin) followed by the image analysis with Xeleris 2.1TM (General Electric).

The RP used are listed below:

1. ^{99m}Tc -pertechnetate in the saline was eluted from $^{99}\text{Mo}/^{99m}\text{Tc}$ generator “GT-4KTM” (NIFKHI, Obninsk, Russia). ^{99m}Tc -pertechnetate was used as a stand-alone RP and as a labeling agent for other RPs. Under physiologic condition it accumulates in thyroid, salivary glands, and stomach.
2. ^{99m}Tc -macroaggregates albumin (MAA) prepared by diluting of the standard lyophilized kit “MacrotekhTM” (Diamed, Moscow, Russia) with ^{99m}Tc -pertechnetate. MAA with the diameter from 10 to 80 μm are usually used in perfusion lung scintigraphy.
3. ^{99m}Tc -dimercaptosuccinic acid (DMSA) prepared by diluting of the standard lyophilized kit “TekhnemekTM” (Diamed, Moscow, Russia) with ^{99m}Tc -pertechnetate.

At normal conditions it accumulates in cells of proximal tubules in kidneys.

4. ^{99m}Tc -phytate colloid (PHC) prepared by diluting of the standard-lyophilized kit “TekhnephytTM” (Diamed, Moscow, Russia) with ^{99m}Tc -pertechnetate. PHC forms colloidal particles with the diameter range of 150 to 1500 nm. It accumulates mostly in reticular endothelial system’s cells in liver and spleen.
5. ^{99m}Tc -ethylenediamine tetramethylene phosphonic acid (EDTMP) prepared by diluting of the standard lyophilized kit “TekhnephorTM” (Diamed, Moscow, Russia) with ^{99m}Tc -pertechnetate. EDTMP is an analogue of MDP, commonly used for bone scan. EDTMP accumulates in growing bone tissue, such as osteoblastic metastatic lesions.

3 Results

3.1 *In Vitro* Studies of Light Emission

For measuring ^{99m}Tc RL and for excluding cross-talk between wells of 96-well black opaque plastic microplate (OptiPlate-96 F, PerkinElmer, Waltham, Massachusetts), one well was filled with 50 MBq of ^{99m}Tc -pertechnetate. All other wells were filled with double-distilled water. The image was acquired with exposure time of 120 s with the following settings of mentioned above parameters $B = 16$, $f/1$, and $\text{FOV} = 13.4$ cm. The average radiance was measured in the regions of interest (ROIs) corresponding to wells and one ROI outside of the microplate, used as the “background” signal. The background radiance was subtracted from every ROI. No significant differences were observed between the ROI, corresponding to wells filled with distilled water (with the average radiance of about 40 p/s/cm²/sr). The light emission was detected only in the ROI corresponding to the well filled with ^{99m}Tc -pertechnetate with the average radiance about 2.5×10^3 p/s/cm²/sr. The empty microplate image was acquired as a “negative control.” The threefold background signal was observed on images with the radioactive material.

After the first part of the experiment, the entire plate was covered by a piece of black paper to absorb any light emission. There were nearly equal average radiances registered in all ROIs (about 45 p/s/cm²/sr), close to the background signal. Therefore, the direct interaction between the light emission from the well with RP and the IVIS charge coupled device (CCD) could be excluded, whereas gamma rays could still pass through the sheet of black paper. The background signal has remained constant.

For testing of higher activities, 500 MBq of ^{99m}Tc -pertechnetate in 0.4 mL of saline solution were added to the central well of the same microplate. Three consequent wells, located next to the central well were filled with MAA saline solution (without ^{99m}Tc -labelling). Remaining wells were filled with double-distilled water. The image was acquired with the same parameters settings as mentioned above. After that, the central well was covered by a 2-mm lead lamella and another image was taken. The light emission was observed in the water-filled wells, located close to the central (the background-corrected average radiance of 1131 p/s/cm²/sr). The slightly higher light emission was observed in the MAA-filled well (1607 p/s/cm²/sr). No RL above the background signal was

Table 1 The average radiance of light emission excited by ^{99m}Tc radiation.

Experiment	Well	Background-corrected average radiance (p/s/cm ² /sr)	Percentage of average radiance (relative to ^{99m}Tc -filled well)
A	^{99m}Tc (500 MBq)	114 130	100%
	Distilled water	1 131	0.99%
	MAA (without ^{99m}Tc)	1 607	1.44%
B	^{99m}Tc (100 MBq)	6937	100%
	Fluorescein (well B)	9820	141.56%
	Fluorescein (well A)	2466	35.55%

detected in other distant wells. The results are shown in Table 1, as Experiment A.

The next test, Experiment B, was to verify the association of observed light emission with gamma radiation. The microplate central well was filled with 100 MBq of ^{99m}Tc -pertechnetate, and two wells located one right next to the central and the other four wells away were filled with fluorescein of equal concentrations. Fluorescein is a luminophore excited by gamma-radiation.²² The image was acquired with the same parameters ($B = 16$, $f/1$, 120 s, no emission filter). The experiment results are also shown in Table 1, as Experiment B and in Fig. 1.

As it was mentioned above, the higher background signal was found with the radioactive source present. To separate this background signal from the direct interaction of gamma-rays with CCD, a gamma source (500 MBq of ^{99m}Tc -pertechnetate) in a lead container was placed outside the FOV. The images with, $B = 16$, $f/1$, without emission filter were taken 120 s before and after placing the source. Then, another

image with the same parameter settings was taken with a small mirror placed in the center of the FOV. The average radiance registered in the ROI in the camera center prior to the gamma source placement was 247 p/s/cm²/sr, with the source present—7082 p/s/cm²/sr, and with the mirror added—11070 p/s/cm²/sr. All three images acquired are shown in Fig. 2.

3.2 Measurement of Decay Half-Life

Measurements of decay half-life and radiance detection efficiency for several PRs were performed using the same black 96-well microplate. The wells were filled with the following RPs (each with relative concentrations as 8:4:2:1): ^{99m}Tc -pertechnetate (column B in Fig. 3), ^{99m}Tc -MAA (column C), ^{99m}Tc -PHC (column D), and ^{99m}Tc -DMSA (column E). Column A contains nearly equal activities of ^{99m}Tc -pertechnetate (15 MBq). Figure 3 demonstrates how differently concentrated RPs were distributed over the microplate. Measurements of the average radiance were performed every 10 min for 16 h. Every image was acquired with exposure time 600 s, $B = 16$, $f/1$, and FOV = 13.4 cm.

The experiment results are shown in Fig. 4. The average radiance of every ROI was corrected for the background signal (which in turn was the average radiance of the ROI corresponding to the space outside of the microplate). As shown in Fig. 5, the background signal was also time- or radioactivity-dependent. Every curve of the radiance decay was approximated to the exponential curve, then decay constant and half-lives were estimated for every RP. The estimates of decay half-lives are presented in Table 2. All values are in agreement with the true half-life for ^{99m}Tc .

3.3 Influence of Radioactivity in Well and Average Radiance

Dependence of the average radiance on radioactivity in well was estimated in the same experiment. Images were acquired with

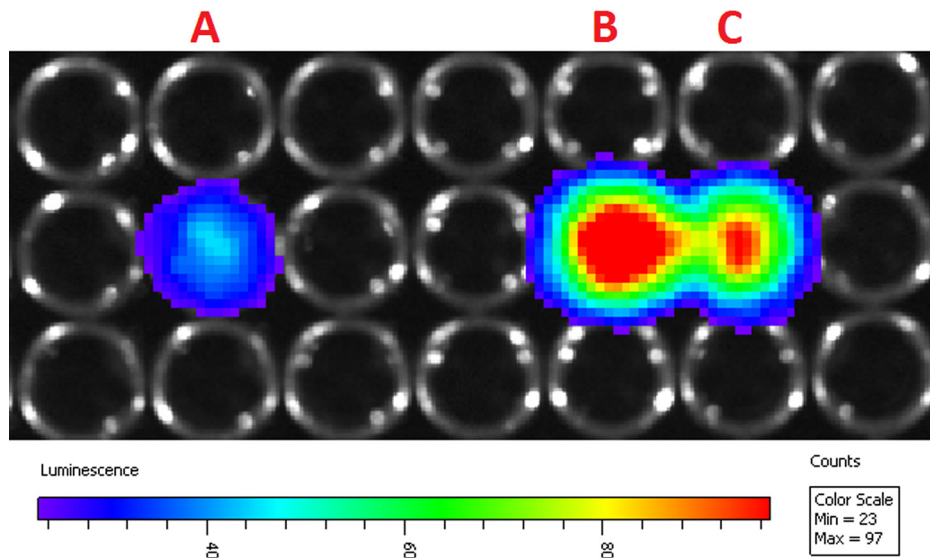


Fig. 1 The excitation of fluorescein with gamma-radiation of Technecium-99m in wells of the black microplate. Well C contains ^{99m}Tc -pertechnetate (100 MBq). Wells A and B contain aqueous solutions of fluorescein in equal concentrations.

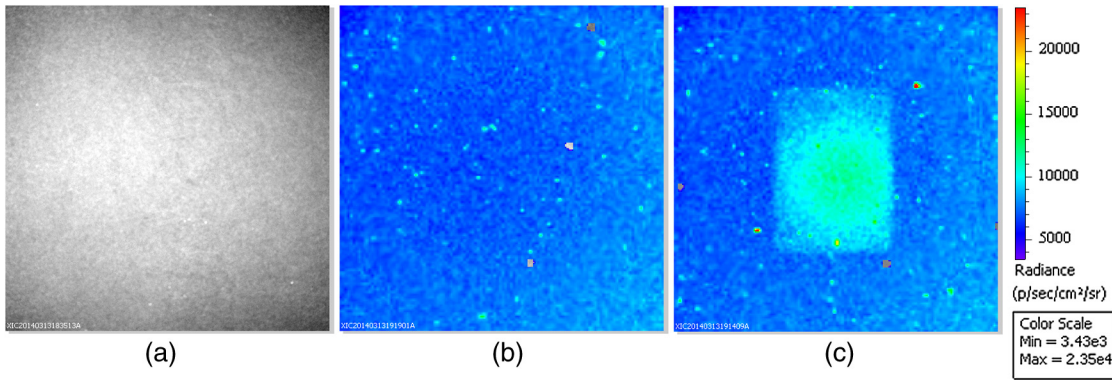


Fig. 2 Background signal investigation. On image (a) there is no gamma-rays source in the camera of IVIS. On image (b) there is a 500 MBq of the ^{99m}Tc -pertechnetate in open lead container, which is placed outside the field-of-view (FOV) in the camera of IVIS (actually, near the right lower corner of image). Image (c) represents the mirror, placed in the center of the camera FOV. There is a same ^{99m}Tc -pertechnetate location.

exposure time 180 s, $B = 16$, $f/1$, and $\text{FOV} = 13.4$ cm. The background-corrected average radiance was determined for every RP-filled well. As shown in Fig. 6, there appear to be a linear dependence between the well radioactivity and the average radiance (R^2 is in the range of 0.89 to 0.99 for different RPs). The highest average radiance was observed for MAA ROL.

3.4 Spectral Characteristics of the Different RPs

The radiance of different wavelengths can be evaluated by using emission filters. Standard emission filters of the IVIS Spectrum CTTM allow estimating a spectrum in wavelength range of 500 to 840 nm with resolution of 20 nm. The 100-MBq solutions of ^{99m}Tc -pertechnetate, MAA, PHY, DMSA, and EDTMP were

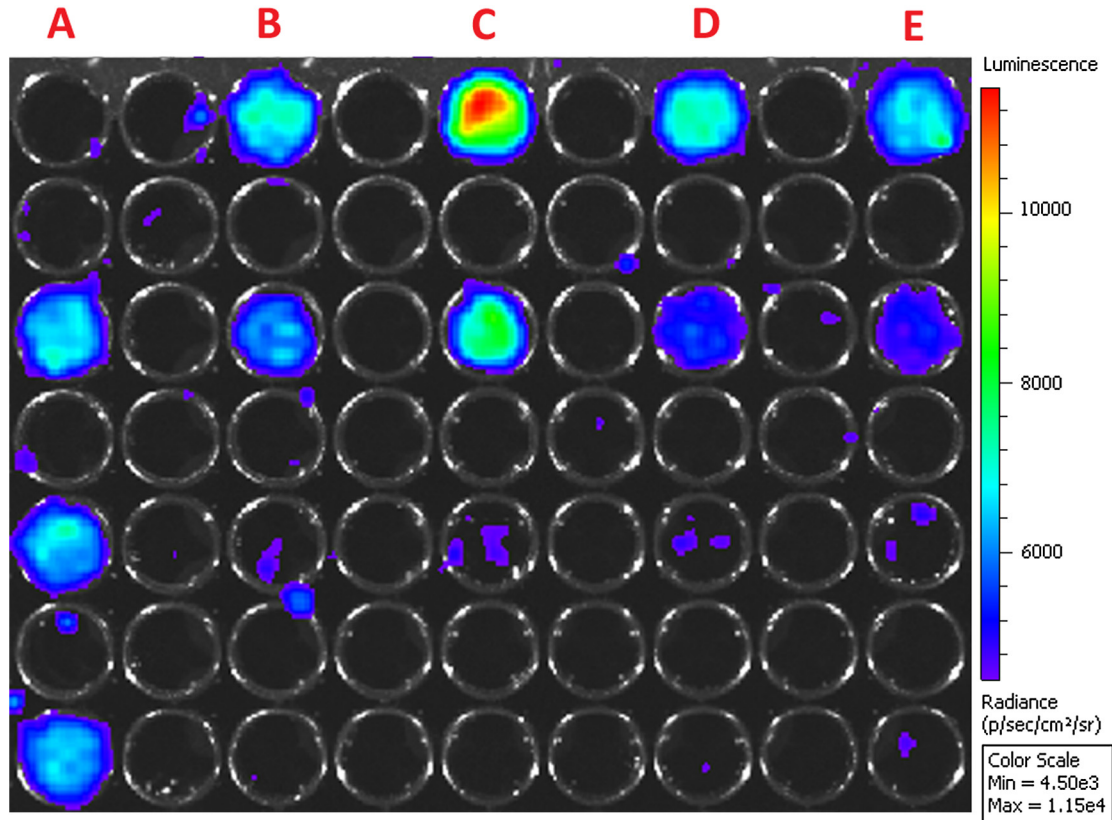


Fig. 3 The black plastic pallet with radiopharmaceuticals (RPs). Wells 3, 5, and 7 of the column A contain nearly equal radioactivity of ^{99m}Tc -pertechnetate (15 MBq). Wells 1,3,5,7 of the columns B, C, D, E contain serial two-fold dilution of the next RPs: ^{99m}Tc -pertechnetate (B), ^{99m}Tc -MAA (C), ^{99m}Tc -PHC (D), ^{99m}Tc -DMSA (E), respectively. Maximum radioactivity (15 MBq) is in the first row, half of that activity—in the third row, etc. All other wells contain equal volume of double-distilled water.

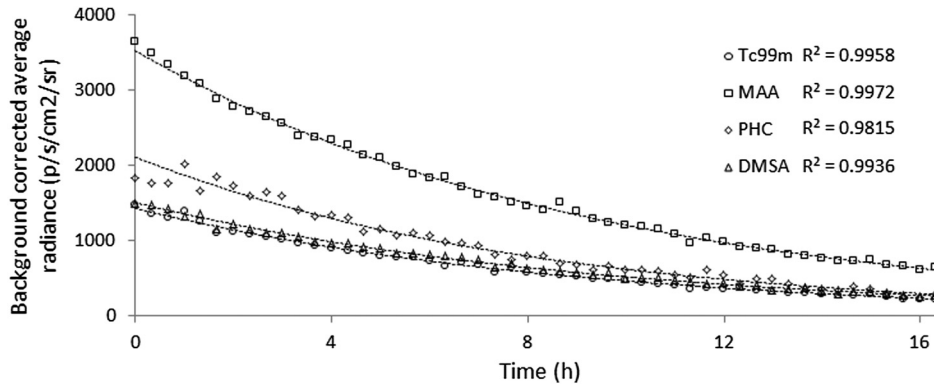


Fig. 4 Time dependence of background-corrected average radiance in regions of interests (ROIs) of ^{99m}Tc (round marker), MAA (square marker), PHY (rhombus marker), and DMSA (triangle marker). All curves are approximated to exponential decay; corresponding coefficients of determination are shown on the right side of figure.

individually shielded in lead containers to avoid cross-talk. Eighteen images were acquired with different filters—each for 600 s, $B = 16$, $f/1$, and $\text{FOV} = 13.4$ cm.

Every datapoint of the average radiance was background and decay corrected. The results are presented in Fig. 7.

3.5 Background Spectrum

The background radiance appeared to be dependent on the emission filter applied. Background radiance measurements were performed with the ROIs placed outside the lead container depiction. The average radiance was determined based on three different experiments with various RP. Eighteen 600-s-long measurements with various emission filters (covered the range of 500 to 840 nm with the resolution of 20 nm) were performed with the following parameter settings: $B = 16$, $f/1$, and $\text{FOV} = 13.4$ cm. The radiance measured for each of the three experiments was normalized by the average radiance value in the wavelength range of 600 to 700 nm (the most linear range) as follows:

$$SI_{\lambda}^n = \frac{SI_{\lambda}}{SI_{600-700 \text{ nm}}},$$

where SI_{λ} is measured signal, SI_{λ}^n is normalized signal.

The data were decay corrected and the results can be seen in Fig. 8.

3.6 In Vivo Intravenous ^{99m}Tc -Colloid Injection

^{99m}Tc -PHY has been chosen for this experiment because it is mostly deposited in macrophage cells of liver and spleen proportionally to the organ perfusion and function activity.

A Wistar-line rat was narcotized by 3% chloral hydrate solution. The abdominal region of the rat was shaved. The luminescence of the animal prior to [Fig. 9(b)] and after injection of 200 MBq of ^{99m}Tc -PHY in the left femoral vein was measured with $B = 16$, $f/1$, $\text{FOV} = 13.4$ cm for 180 [Fig. 9(c)] and 600 s [Fig. 9(d)].

Intensive luminescent signal was detected near the injection site, whereas no signal in the liver region was observed. Additionally, there was a prompt increase in the background signal right after the RP administration.

3.7 Scintillator Luminescence

Since no light emission was detected in the liver region in the experiment above, RP accumulation in liver needed to be proved. The same animal was measured with NaI(Tl) scintillator (S114455, Gamma Technical Corporation, Budapest, Hungary) 40 mm in diameter and 2.5-mm thick. The image was acquired

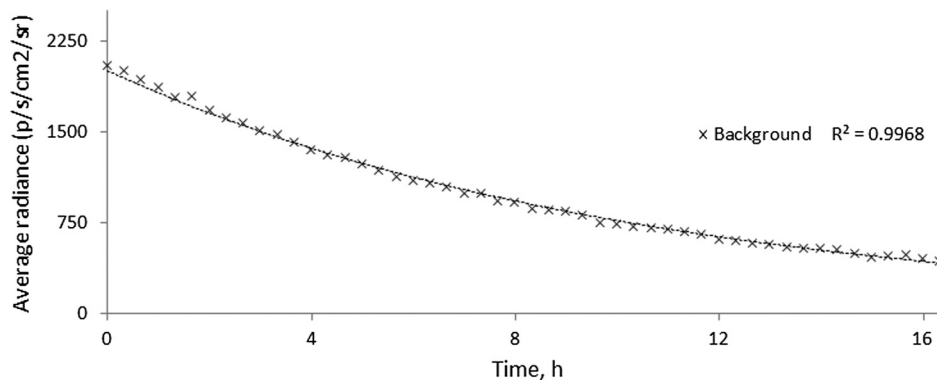


Fig. 5 Time dependence of average radiance in background ROI signal. Curve is approximated to exponential decay; corresponding coefficient of determination is shown on the right side of the figure.

Table 2 Calculated half-lives for ^{99m}Tc -pertechnetate, MAA, PHY, and DMSA.

ROI	Half-life
^{99m}Tc	6:10
MAA	6:28
PHC	5:40
DMSA	6:31
Background	7:09

for 2 s with the following parameter settings: $B = 2$, $f/1$ in 22.9-cm FOV. Eighteen measurements of the luminescence of the scintillation crystal of different regions were merged into the one image (Fig. 10). The maximal intensity is seen to be concentrated in the liver region of the animal. That in turn confirms an expected location for accumulation of the injected RP.

The RP accumulation was studied for ^{99m}Tc -PHC in the IVIS with the scintillator positioned over the liver region of the animal. A similar experiment was performed with a conventional gamma-camera in order to verify pharmacokinetics.

In the first part of experiment, a narcotized rat injected with 200 MBq of the ^{99m}Tc -PHC in the femoral vein, was measured using the IVIS camera with NaI(Tl) scintillator positioned over the liver region. A sequence of images was taken with next parameter settings: $B = 16$, $f/1$, FOV = 13.4 cm and exposure time of 3 s and with 9 s in between the images. The measured average radiance of the scintillator ROI for every datapoint in time is plotted on the graph [Fig. 11(a)].

In the second part of experiment, an animal was placed between two detectors of the gamma-camera (Infinia 4 Hawkeye™, General Electric, Milwaukee, Wisconsin). A sequence of images was taken with the exposure time of 15 s per image and with no delay between frames. The image matrix used was 512×512 pixels. Measured counts in the liver ROI for every time point was plotted on the same graph [Fig. 11(a)]. Static scintigraphy of the animal is provided in Fig. 11(b). The ^{99m}Tc -PHC accumulation location was also verified with the SPECT/CT study (data not shown).

3.8 Glass Scintillator for ^{99m}Tc -RP Optical Imaging

Borosilicate glass (a Petri dish) was also tested as a scintillator. The parameter settings were: $B = 16$, $f/1$, FOV = 13.4 cm and exposure time of 180 s. A high-luminescent signal was again detected in the liver region. The high radiance was also observed in the walls of the Petri dish (Fig. 12).

The luminescence spectral characteristics were measured in the wavelength range of 500 to 840 nm. Again 18 emission filters were used with resolution of 20 nm. One image per filter was acquired for 600 s with the following parameter settings: $B = 16$, $f/1$, ad FOV = 13.4 cm. The data obtained are presented in Fig. 13.

4 Discussion

4.1 Interaction between Gamma-Radiation and CCD

The *in vitro* study results showed that ^{99m}Tc -based radiotracers produce weak light emission in the visible wavelength range. This RL is much weaker, than Cherenkov light emission of positron-emitting isotopes. Thus, ^{99m}Tc -induced visible light emission was not seen in studies of Xu et al.,¹⁰ Liu et al.,¹⁹ and Robertson et al.²

The experiments with a mirror and black paper (see Sec. 3.1) led to conclusion that the direct interaction of gamma-rays and the CCD did not result in a detectable signal. However, if sources of intensive radiation are present then some “hot spot” unwanted features become noticeable (see Fig. 2).

4.2 Radioluminescent Nature of the Light Emission In Vitro

The light emission appears associated with the RL of water, as described in Refs. 23 and 24. The RL of known luminophores,²⁵ such as cyclic compounds or metal-organic complexes, contributes to this light emission too. The radioluminescent theory is supported by the experiment with different RPs. Albumin aggregates, containing a huge amount of cyclic aminoacids, emit more intensive radiance than other RPs including metalloorganic compounds, such as DMSA and EDTMP (Figs. 6 and 7). The known luminophore, fluorescein, has shown high light emission even in the distant well (see Fig. 1). This in turn suggests that this luminescence is associated with

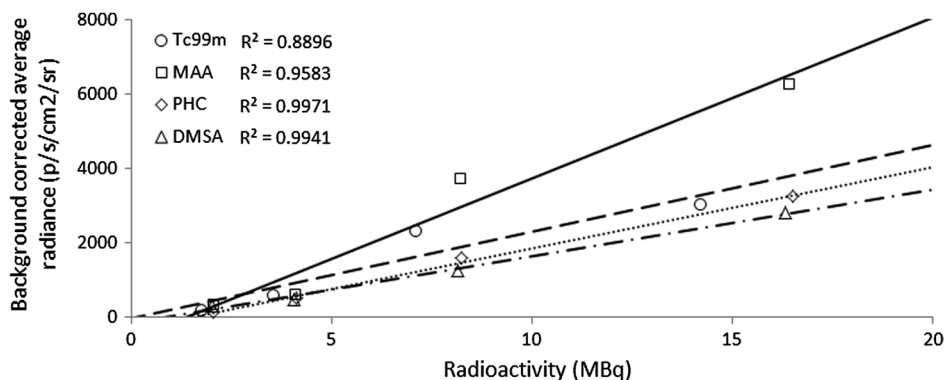


Fig. 6 Average radiance dependency on radioactivity in well. There are linear trend lines drawn for every RP; coefficient of determination is shown on the left side of the figure.

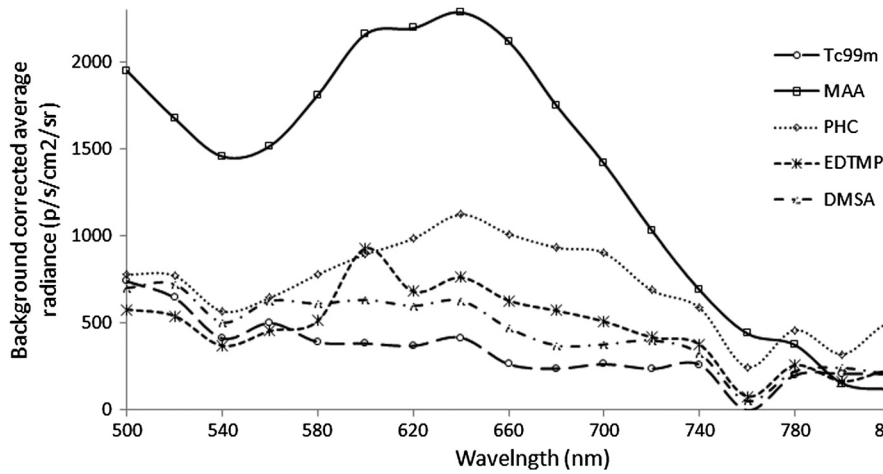


Fig. 7 Spectral distribution of background-corrected average radiance. At start point of experiment, radioactivity of every RP was 100 MBq. Solid line with square marker represents intensity of ^{99m}Tc -MAA, dotted line— ^{99m}Tc -PHC, short dashed line— ^{99m}Tc -EDTMP, long dotted line— ^{99m}Tc -pertechnetate, dash-dotted line— ^{99m}Tc -DMSA.

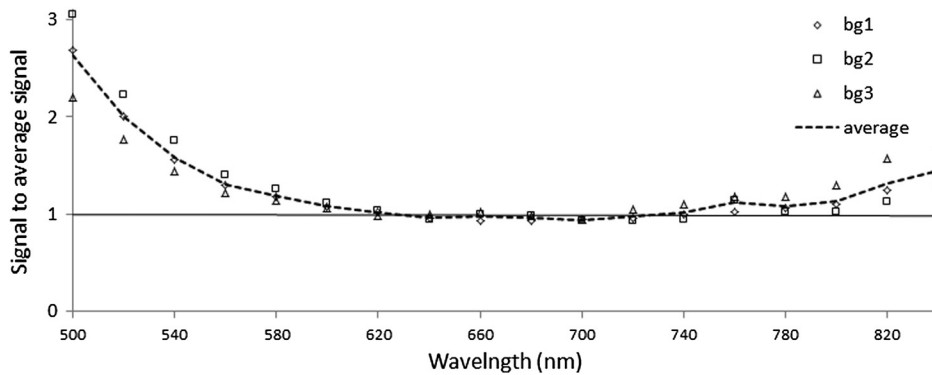


Fig. 8 Spectral characteristics of normalized background signal for three measurements (bg1, bg2, and bg3) and their average values (dashed curve).

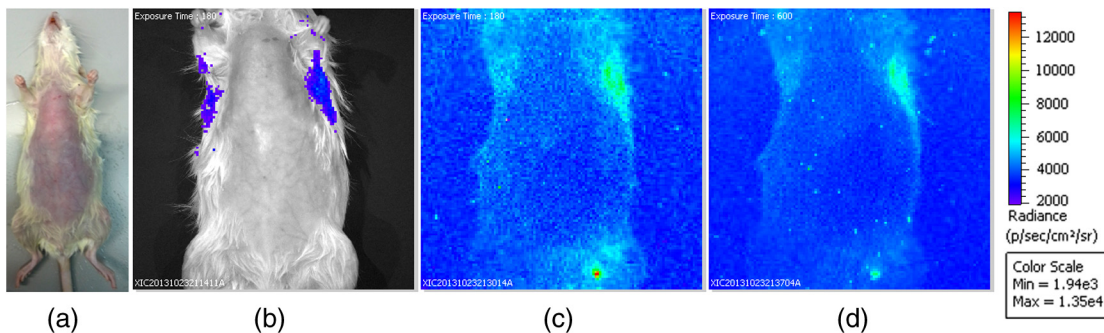


Fig. 9 Conventional photograph of rat (a) and fused images from IVIS (photograph and luminescence) before (b) and after (c and d) ^{99m}Tc -PHC injection. Images (b), (c), and (d) are presented in the same radiance window. For (b) and (c) exposure time is 180 s, for (d) 600 s, other image acquisition parameters are same.

gamma-rays. These findings were used in scintillators based on aromatic dyes, such as fluorescein.²²

4.3 Question about Cherenkov Light Emission Probability

This kind of luminescence is induced by gamma-rays of technetium-99m. Unlike Cherenkov light emission, the RL is

produced by excitation of an orbital electron and consequent return to its ground state with light emission. Cherenkov light emission is caused by a charged particle (e.g., electron or positron) traveling in media with a velocity exceeding the speed of light. The speed of light in vacuum and in media is related by the refractive index of the media. The refractive index of water is 1.33, so the threshold energy for CR, produced by electrons, is about 264 keV. The refraction coefficient for

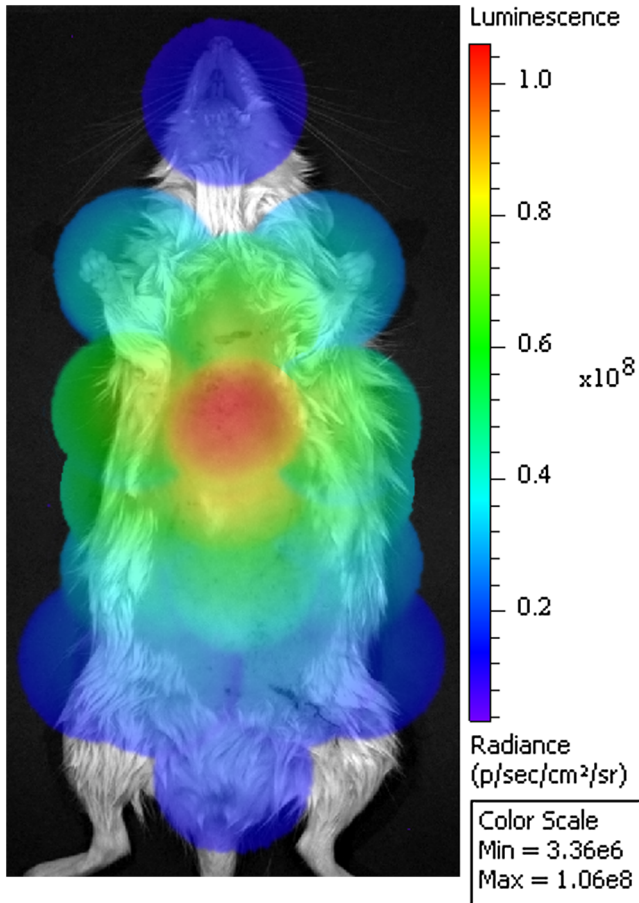


Fig. 10 Luminescence of the scintillation crystal in 18 different regions, which are summed in one image and fused with a photograph of an animal. Radiance window is the same and shown on the right side of image. The injected RP is ^{99m}Tc -PHC.

borosilicate glass is about 1.5, and the threshold energy of electron for Cherenkov emission to occur is 174 keV. Maximum ^{99m}Tc energy threshold for gamma-radiation is 142 keV, so the highest energy of an electron, which could be released by the photoelectric effect, is below 140 keV. However, in materials with the refractive index greater than 1.62, Cherenkov photons emission might contribute to detected signal.

Additionally, the light spectral distribution in our case confirms the RL as the origin of the light emission the intensity of Cherenkov light emission is reverse proportional to the squared wavelength of the visible light. Whereas the RL spectral distribution is different and its maximum intensity does not corresponds to the wavelength of light. Figure 7 demonstrates the RL spectral distribution with the maximum at about 650 nm for MAA and PHC.

4.4 Decay Half-Life and Air Radioluminescence

A CCD is a detector sensitive enough to detect weak light emission, even with the source activity is about 1 MBq (Fig. 6). The calculated half-life of ^{99m}Tc for different RPs approximates at 6 h. It should be noted that the background signal decayed with half-life about 7 h. Despite of such difference we assume that it is also associated with ^{99m}Tc decay. Considering this along with the spectral distribution of the background radiance and the experiment with the mirrored light, we assume that there might be the RL of air. This type of RL may be associated with the interaction between ^{99m}Tc gamma-rays and nitrogen atoms in the air. The latter element has a peak in blue range of the visible light, as stated in Ref. 26. The RL of air might contribute into detected signal, especially when a large quantity of radioactivity is present. This in turn may lead to a smaller signal-to-noise ratio in further studies. Also Fahimian et al.²⁷ referred to the air scintillation caused by lower energy (about 50 to 60 keV) photons from x-ray tube.

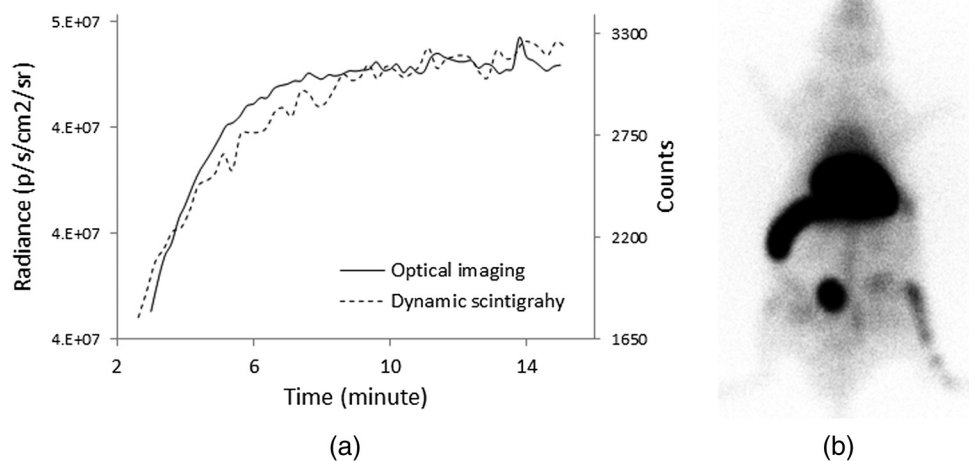


Fig. 11 Comparison of the pharmacokinetics of liver accumulation of the ^{99m}Tc -PHC. Data for graph (a) was obtained by means of optical imaging (solid line, left vertical axis) and dynamic scintigraphy (dashed line, right vertical axis). (b) Static scintigraphy of rat after the dynamic study, liver and spleen are clearly visualized. The round structure in the lower abdominal region is believed to be an injection site artifact.

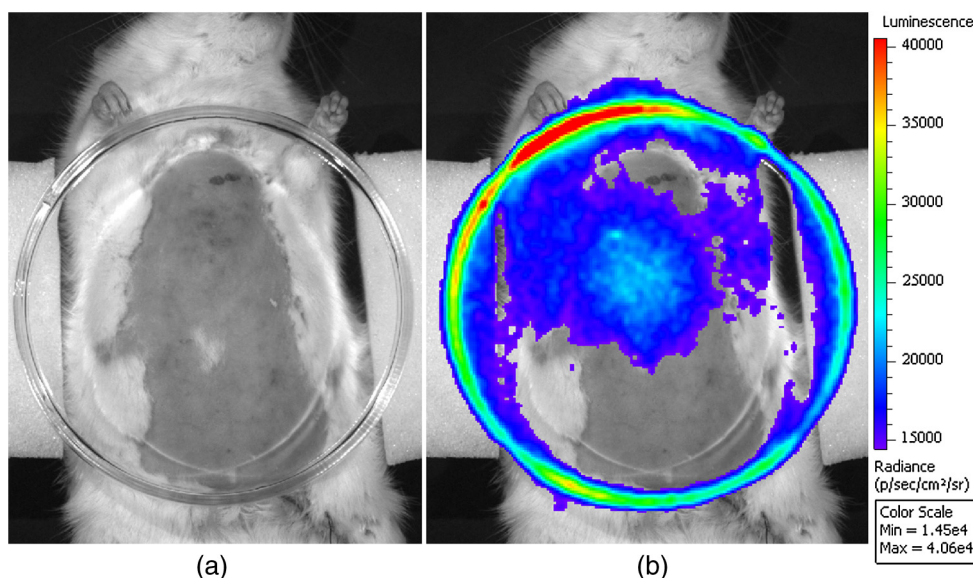


Fig. 12 Luminescence of the Petri dish placed above a rat with ^{99m}Tc -PhC injected. (a) A photograph, and (b) a fused image.

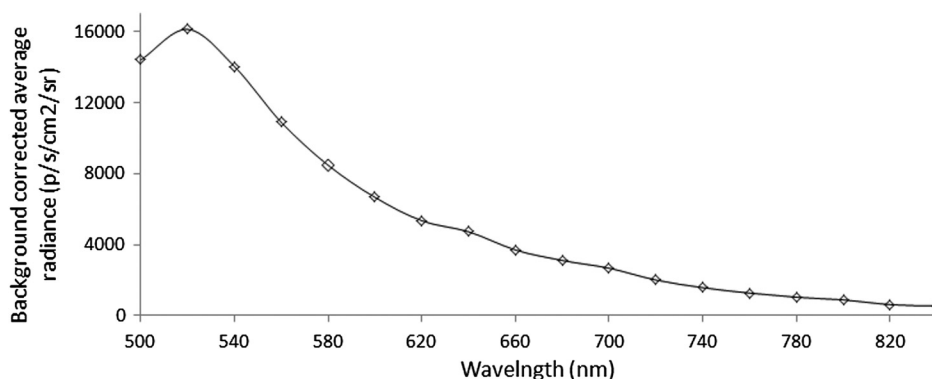


Fig. 13 Background-corrected average radiance from borosilicate glass scintillator.

4.5 *In Vivo Findings*

The primary purpose of the *in vivo* experiment was to assess feasibility of optical visualization of liver with ^{99m}Tc -phytate colloid. It was assumed that ^{99m}Tc -PhC will accumulate in liver and hence it would be possible to perform organ visualization. However, there was no significant RL observed in the region of liver. Images acquired for 180 s and for 600 s exposure time are shown in Fig. 9. It was also noticed that background RL was significantly higher after the RP injection compared with that prior to the injection. A significantly high RL, corresponding to some amount of RP, was detected in the small region near the injection site. The experiment with scintillators proved that ^{99m}Tc -PhC is accumulated by the liver of the animal.

The dynamic study of ^{99m}Tc -PhC accumulation in liver should provide semi-quantitative analysis of RP's pharmacokinetics. It is seen, that uptake curves obtained from the optical imaging system and the gamma-camera are very similar.

A possible reason for an RL signal absent from the liver region may relate to high absorption of the visible light by animal tissues. In addition, the RP specific activity in liver was

about 20 MBq/g of tissue, which is lower than the evaluated ^{99m}Tc specific activity of in thyroid in Boschi et al.²¹

It is known that certain types of glass could be used as scintillators, for example a borosilicate glass.²⁸ Using a Petri dish made of borosilicate glass, it is possible to find a distribution of radioactivity in small animal. So, a CCD could acquire an image of certain types of inexpensive scintillators, e.g., some types of glass and plastic.

4.6 *Limitations*

Despite some promising findings, there are some limitations for the direct application of ^{99m}Tc RL in preclinical investigations. First of all, spatial resolution and quality of the images should be better. This would be difficult to implement in IVIS cameras. However, new CCD-based gamma-camera or SPECT, can be designed with paying attention to scintillator selection, using optical fibers as light guides and other technical features in order to significantly improve the image quality.

5 Conclusions

The RL of fluids induced by ^{99m}Tc-based tracers could be detected by preclinical optical imaging devices with CCD. Intensity and spectral distribution of that RL depends on a surrounding fluid and the presence of known luminophores in it. The visible light emission is related with the RL and not with CR. Weak air luminescence influencing background signal is presumably due to nitrogen RL in presence of radiation source.

As it was shown the visualization of small animals in pre-clinical studies including that with scintillation detectors is quite possible.

The RL imaging of ^{99m}Tc-based tracers may be applied in certain cases, when gamma-camera or SPECT for animals cannot be used. The application of collimators affront of scintillators may improve imaging spatial resolution in the expense of detection efficiency that in turn might require using higher activity RP injections.

Acknowledgments

We would like to express our great appreciation to Dariya D. Namestnikova for help with animal handling. We also want to offer our special thanks to Maxim A. Abakumov for his valuable suggestions over the course of the work. Last, but not least, we are particularly grateful for the invaluable assistance and support given by Andrey V. Mozhayev.

References

1. E. Fernandes et al., "Positron emitting tracers in pre-clinical drug development," *Curr. Radiopharm.* **5**(2), 90–98 (2012).
2. R. Robertson et al., "Optical imaging of Cerenkov light generation from positron-emitting radiotracers," *Phys. Med. Biol.* **54**(16), N355–N365 (2009).
3. P. A. Cerenkov, "Visible emission of clean liquids by action of γ radiation," *Dokl. Akad. Nauk SSSR* **2**(8), 451–454 (1934).
4. J. V. Jelley, *Cerenkov Radiation, and its Applications*, pp. 2–3, Pergamon Press, New York (1958).
5. A. E. Spinelli et al., "Cerenkov radiation allows in vivo optical imaging of positron emitting radiotracers," *Phys. Med. Biol.* **55**(2), 483–495 (2010).
6. G. S. Mitchell, R. K. Gill, and S. R. Cherry, "Comments on 'Cerenkov radiation allows in vivo optical imaging of positron emitting radiotracers'," *Phys. Med. Biol.* **55**(18), L43–L44 (2010).
7. D. Thorek et al., "Cerenkov imaging—a new modality for molecular imaging," *Am. J. Nucl. Med. Mol. Imaging* **2**(2), 163–173 (2012).
8. Y. Xu et al., "Proof-of-concept study of monitoring cancer drug therapy with cerenkov luminescence imaging," *J. Nucl. Med.: Off. Publ., Soc. Nucl. Med.* **53**(2), 312–317 (2012).
9. Y. Xu et al., "Cerenkov Luminescence Imaging (CLI) for cancer therapy monitoring," *J. Visualized Exp.: JoVE* **69**, e4341 (2012).
10. Y. Xu, H. Liu, and Z. Cheng, "Harnessing the power of radionuclides for optical imaging: Cerenkov luminescence imaging," *J. Nucl. Med.: Off. Publ., Soc. Nucl. Med.* **52**(12), 2009–2018 (2011).
11. G. Lucignani, "Cerenkov radioactive optical imaging: a promising new strategy," *Eur. J. Nucl. Med. Mol. Imaging* **38**(3), 592–595 (2011).
12. A. E. Spinelli and F. Boschi, "Unsupervised analysis of small animal dynamic Cerenkov luminescence imaging," *J. Biomed. Opt.* **16**(12), 120506 (2011).
13. A. E. Spinelli et al., "Multispectral Cerenkov luminescence tomography for small animal optical imaging," *Opt. Express* **19**(13), 12605–12618 (2011).
14. R. S. Dohager et al., "Cerenkov radiation energy transfer (CRET) imaging: a novel method for optical imaging of PET isotopes in biological systems," *PLoS One* **5**(10), e13300 (2010).
15. F. P. Lopes et al., "^{99m}Tc-Anti-TNF-alpha scintigraphy: a new perspective within different methods in the diagnostic approach of active Graves ophthalmopathy," *Clin. Nucl. Med.* **37**(11), 1097–1101 (2012).
16. A. M. Wallace et al., "Comparative evaluation of [(99m)tc]tilmanocept for sentinel lymph node mapping in breast cancer patients: results of two phase 3 trials," *Ann. Surg. Oncol.* **20**(8), 2590–2599 (2013).
17. M.-M. Bé et al., "Table of Radionuclides," in *Monographie BIPM-5*, Bureau International des Poids et Mesures, Sèvres (2013).
18. A. E. Spinelli et al., "Optical imaging of Tc-99m-based tracers: in vitro and in vivo results," *J. Biomed. Opt.* **16**(11), 116023 (2011).
19. H. Liu et al., "Molecular optical imaging with radioactive probes," *PLoS One* **5**(3), e9470 (2010).
20. F. Boschi et al., "Combined optical and single photon emission imaging: preliminary results," *Phys. Med. Biol.* **54**(23), L57–L62 (2009).
21. F. Boschi et al., "Small-animal radionuclide luminescence imaging of thyroid and salivary glands with Tc99m-pertechnetate," *J. Biomed. Opt.* **18**(7), 76005 (2013).
22. M. Nikl et al., "Scintillators based on aromatic dye molecules doped in a sol-gel glass host," *Appl. Phys. Lett.* **86**(10), 101914 (2005).
23. T. I. Quickenden and S. S. Que Hee, "The luminescence of water excited by ambient ionizing radiation," *Radiat. Res.* **46**(1), 28–35 (1971).
24. D. N. Sitharamarao and J. F. Duncan, "Molecular excitation of water by γ -irradiation," *J. Phys. Chem.* **67**(10), 2126–2132 (1963).
25. B. M. Krasovitskiy and B. M. Bolotin, *Organic Luminophores*, 2nd ed., pp. 23–24, Khimiya, Moscow (1984).
26. M. D. Tarasov et al., "An air scintillator," *Instrum. Exp. Tech.* **54**(3), 320–322 (2011).
27. B. Fahimian et al., "Seeing the invisible: direct visualization of therapeutic radiation beams using air scintillation," *Med. Phys.* **41**(1), 010702 (2014).
28. R. J. Ginther and J. H. Schulmian, "Glass scintillators," *IRE Trans. Nucl. Sci.* **5**(3), 92–95 (1958).

Anton K. Kondakov is a resident in radiology at the Pirogov Russian National Research Medical University (RNRMU). He graduated from RNRMU in 2012 majoring in medical biophysics. His current research interests include nuclear medicine imaging.

Ilya L. Gubskiy is a resident in radiology at the Russian Medical Academy of Postgraduate Education. He graduated from RNRMU in 2013, majoring in medical biophysics. His current research interests include molecular imaging and MRI.

Igor A. Znamenskiy is a professor in the Radiology Department at the Pirogov Russian National Research Medical University and head of the Department of Radionuclide Imaging at Central Clinical Hospital of RAS. He graduated from the 2nd Moscow Medical Institute in 1988. He was granted a Doctor of Sciences degree in 2008 from Higher Attestation Commission in Russia. His current research interests include nuclear medicine imaging.

Vladimir P. Chekhonin is a head of the Department of Fundamental and Applied Neurobiology in Serbsky Institute for Social and Forensic Psychiatry and Chairperson of the Department of Medicinal Nanobiotechnologies, Faculty of Biomedicine in Pirogov Russian National Research Medical University. He was granted a Doctor of Sciences degree in 1989. His current research interests include nanobiotechnology and targeted drug delivery.